Discrimination between Alpha-Synuclein Protein Variants with a Single Nanometer-Scale Pore

Mazdak Afshar Bakshloo, Safia Yahiaoui, Matthieu Bourderioux, Régis Daniel, Manuela Pastoriza-Gallego, John Kasianowicz, Abdelghani Oukhaled

Discrimination between Alpha-Synuclein Protein Variants with a Single Nanometer-Scale Pore

Mazdak Afshar Bakshloo, Safia Yahiaoui, Matthieu Bourderioux, Régis Daniel, Manuela Pastoriza-Gallego, John Kasianowicz, Abdelghani Oukhaled

Discrimination between Alpha-Synuclein Protein Variants with a Single Nanometer-Scale Pore

Mazdak Afshar Bakshloo, Safia Yahiaoui, Matthieu Bourderioux, Regis Daniel, Manuela Pastoriza-Gallego, John J. Kasianowicz,* and Abdelghani Oukhaled*

ABSTRACT: Alpha-synuclein is one of several key factors in the regulation of nerve activity. It is striking that single- or multiple-point mutations in the 140-amino-acid-long protein can change its structure, which leads to the protein's aggregation and fibril formation (which is associated with several neurodegenerative diseases, *e.g.*, Parkinson's disease). We recently demonstrated that a single nanometer-scale pore can identify proteins based on its ability to discriminate between protease-generated polypeptide fragments. We show here that a variation of this method can readily discriminate between the wild-type alpha synuclein, a known deleterious point mutation of the glutamic acid at position 46 replaced with a lysine (E46K), and a post-translational modification (*i.e.*, tyrosine Y39 nitration).

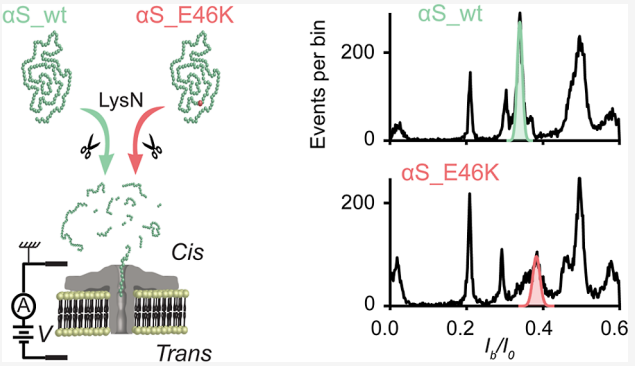

KEYWORDS: *alpha-synuclein, nanopores, Parkinson's disease, protein identification, post-translational modifications*

INTRODUCTION

Alpha-synuclein (αS) is a protein located primarily in neurons,[1−3] where it aids in the regulation of synaptic vesicle trafficking and neurotransmitter release.[4,5] In dysfunctional states, it is associated with several neurodegenerative diseases (synucleinopathies), including Parkinson's disease (PD),[6,7] multiple system atrophy,[8−11] dementia with Lewy bodies (DLB),[12−16] and others.[17,18] In these cases, αS, which is intrinsically disordered,[19] typically accumulates and aggregates into fibril structures[20−24] in Lewy bodies.[3] It is the latter form that induces cytotoxic effects, which are assumed to be responsible, in part, for the symptoms noted above. Some evidence suggests that αS can interact with relatively short amyloidogenic proteins (*e.g.*, Aβ40 and Aβ42).[25,26]

Alpha synuclein's sequence is highly conserved in many species,[27−29] and in humans it is composed of 140 amino acids.[30,31] A rather striking finding is that a point mutation of the guanosine to adenosine at position 209 (G209A) in the SNCA gene encoding for αS, which causes an A53T amino acid change in the N-terminal repeat segment of the protein, is associated with PD.[32−34] After the initial study, it was shown that additional missense mutations of αS, including A53E,[35] A30P,[36] and E46K,[37] were linked to PD as well.

We previously demonstrated that an ion channel formed by aerolysin (AeL) can discriminate between different proteins based on how their protease-cleaved fragments partition into the channel's nanometer-scale pore and thereby reduce its ionic conductance.[38,39] For example, trypsin-induced fragments from three different full-length proteins (myoglobin, lysozyme, and cytochrome C, with molecular masses between 12 and 16.9 kg mol^{-1}) produce ionic current signal patterns that act as characteristic fingerprints of each protein. Here, we show that the method can also distinguish between proteolytic fragments from wild-type αS, one of the deleterious point mutants mentioned above (E46K), and a post-translational modification (PTM) of αS (Y39 nitration). This method should be versatile because the use of multiple proteases allows the targeted cleavage of the αS protein into detectable peptide fragments of desired length carrying the mutation(s) or PTM(s) of interest, thereby permitting the discrimination of various forms of αS protein.

RESULTS

The primary sequence of full-length wild-type (*i.e.*, native) αS (αS_wt) is shown in Scheme 1. To produce the desired enzyme-induced cleavage fragments for αS_wt and the single-point mutant version (αS_E46K), we used the recombinant zinc metalloprotease LysN from Grifola frondose, which cleaves proteins at the amino terminus side of lysine

Received: March 11, 2023
Accepted: May 18, 2023

Scheme 1. Full Length Human α-Synuclein Sequence[a]

```
         10         20         30         40         50
MDVFMKGLSK AKEGVVAAAE KTKQGVAEAA GKTKEGVLYV GSKTKEGVVH
         60         70         80         90        100
GVATVAEKTK EQVTNVGGAV VTGVTAVAQK TVEGAGSIAA ATGFVKKDQL
        110        120        130        140
GKNEEGAPQE GILEDMPVDP DNEAYEMPSE EGYQDYEPEA
```

[a]The sequence of 140 amino acids in αS, with the first proteolytically cleaved fragment of interest (highlighted in yellow) and the single-point amino acid mutation studied here (αS_E46K, emphasized in red).

residues.[40−42] Thus, LysN cleavage of wild-type αS would theoretically create 16 total polypeptides with varying numbers of amino acid residues and composition, of which 13 are unique (Table 1). Note that one of these fragments, which

Table 1. LysN Cleavage Products of Wild-Type αS (αS_wt)[a]

Length	Sequence	Mass (g mol^{-1})	Charge @ pH 7.5
1	K	146.2	1
2	KA	217.27	1
2	KT	247.29	1
2	KT	247.29	1
2	KT	247.29	1
2	KT	247.29	1
4	KGLS	403.48	1
5	MDVFM	641.8	-1
5	KDQLG	559.62	0
9	KEGVVAAAE	872.97	0
9	KQGVAEAAG	829.91	0
9	KEGVLYVGS	951.09	0
13	KEGVVHGVATVAE	1295.46	-1
16	KTVEGAGSIAAATGFV	1478.67	0
20	KEQVTNVGGAVVTGVTAVAQ	1928.17	0
39	KNEEGAPQEGILEDMPVDPD NEAYEMPSEEGYQDYEPEA	4416.59	-13

[a]The protease cleavage fragment in which the point mutation E46K occurs is highlighted in yellow, and the two amino acids are emphasized in red colored text. The three 9-amino-acid-long fragments highlighted in light orange are discussed later in this study.

contains 13 amino acids highlighted in yellow (residues 45 to 57, inclusive), is where the E46K point mutation considered here would be located. Thus, as we demonstrate below, the ability to discriminate between the two versions of this particular fragment, αS_wt and αS_E46K, is a key to differentiate between these versions of the full-length protein.

The physical properties of this fragment's two variants are listed in Table 2. Note that the $(\alpha S\_wt)_{13}$ fragment has 13 amino acids, whereas $(\alpha S\_E46K)_{12}$ has 12, because the latter's full-length protein includes an additional LysN cleavage site at residue 46. The net charges on each of the polypeptide fragments are −1 and 0 for the αS variants $(\alpha S\_wt)_{13}$ and $(\alpha S\_E46K)_{12}$, respectively.

Table 2. Properties of the Two α-Synuclein Fragments Studied Here[a]

Fragment	Length (amino acids)	Sequence	Mass (g mol^{-1})	Charge @ pH 7.5
$(\alpha S\_wt)_{13}$	13	KEGVVHGVATVAE	1295.46	-1
$(\alpha S\_E46K)_{12}$	12	KGVVHGVATVAE	1166.32	0

[a]The altered amino acid in the point mutant is highlighted in red colored text.

Because protein-based nanopores can differentiate between slightly different molecular species,[43−60] including proteins,[38,39,61] we used the nanometer-scale pore formed by the protein *Aeromonas hydrophila* AeL[62,63] in an attempt to discriminate between the two αS polypeptides in Table 2.

In the protein nanopore-based analytical method,[47] an ion channel is formed in a planar lipid bilayer membrane, and the target species are typically added to one of the two aqueous electrolyte solutions bathing the membrane. Individual molecules that enter the pore transiently reduce the ionic current due to volume exclusion and, in certain instances to the reversible binding of mobile ions to the molecules.[49] The degree by which the single channel current is reduced, and the distribution of residence (or dwell) times for the molecules in the pore provide information about the target molecules' physical and chemical properties.[49] The relatively long dwell times of single polypeptides in the pore are a consequence of the interaction between the two.

We first show how enzymatically cleaved fragments of wild-type αS (αS_wt) and the E46K single-point mutant version (αS_E46K) interact with a single AeL nanopore. Figure 1A illustrates schematically that the LysN-induced cleavage of

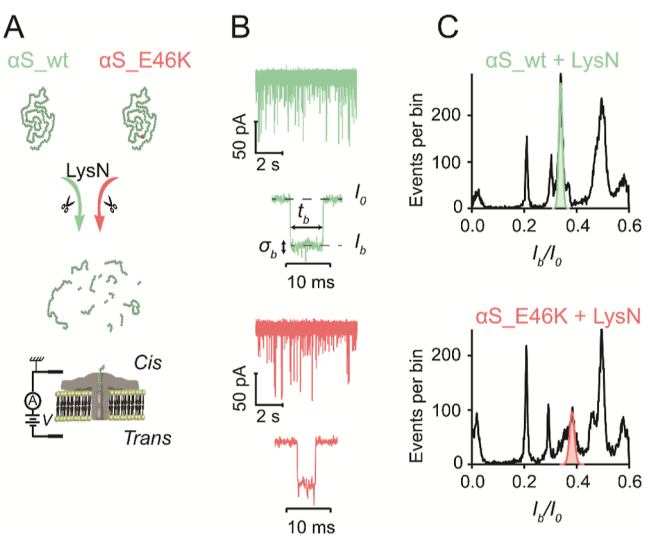

Figure 1. Nanopore-based discrimination of protease fragments of wild-type α-synuclein (αS_wt) and a point mutant version of the protein (αS_E46K). (A) Cleavage of either full length αS_wt or αS_E46K by protease LysN produces well-defined polypeptide fragments. Polypeptide fragment samples of either αS_wt or αS_E46K are added to the electrolyte solution surrounding one side (*cis*) of an AeL nanopore. A transmembrane voltage V drives fragments into the pore and thereby reduces the pore's ionic conductance. (B) Protease-induced fragments of αS_wt or αS_E46K cause short-lived reductions in the ionic current (typical single blockade events for each of the samples are shown); I_0, I_b, σ_b, and t_b are the mean open current, the mean blocked current, the standard deviation of the blocked current, and dwell time for each event, respectively. (C) Histogram of the I_b/I_0 values for the cleaved samples of αS_wt (top) or αS_E46K (bottom). The colored peaks correspond to a Gaussian fit to those segments of the data. All data were recorded at T = 22 °C, [KCl] = 2.5 M, [$CaCl_2$] = 1 M, [HEPES] = 25 mM, pH 7.5, and the transmembrane potential was V = +80 mV. The data shown here are for a single experiment, but the results were highly reproducible (n = 3).

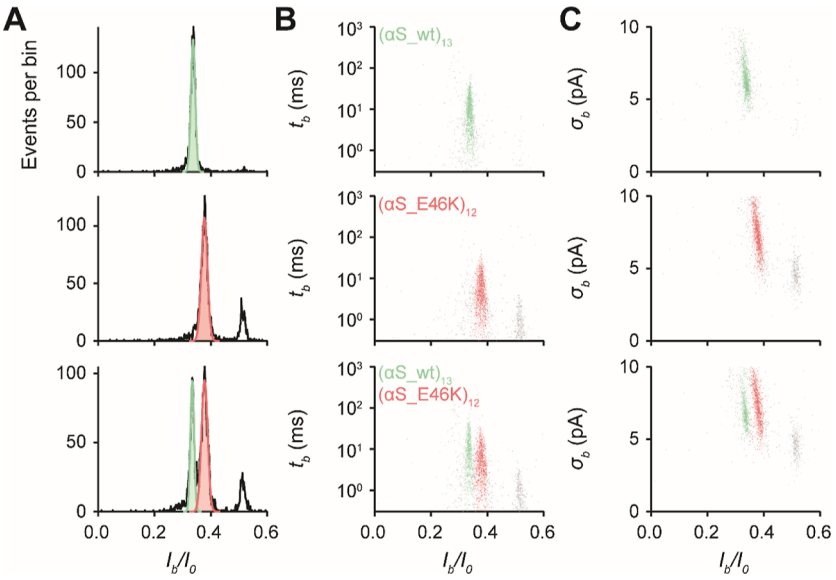

Figure 2. Nanopore-based discrimination of the synthetic short polypeptides $(\alpha S\_wt)_{13}$ and $(\alpha S\_E46K)_{12}$ (Table 2). (A) Single channel ionic current blockade value histograms, (B) dwell time (t_b) *vs* current blockade value (I_b/I_0) event plots, and (C) blocked ionic current standard deviation event plots for $(\alpha S\_wt)_{13}$ only (top); $(\alpha S\_E46K)_{12}$ only (middle); or an equimolar mixture of both $(\alpha S\_wt)_{13}$ and $(\alpha S\_E46K)_{12}$ polypeptides in the same sample (bottom). Gaussian fits to the predominant single peaks for the $(\alpha S\_wt)_{13}$ (green) or $(\alpha S\_E46K)_{12}$ (red) samples are shown. All data were recorded at T = 22 °C, [KCl] = 2.5 M, [$CaCl_2$] = 1 M, [HEPES] = 25 mM, pH 7.5, and the transmembrane potential was V = +80 mV. These data were obtained in single experiments but were highly reproducible in n > 3 replicates.

either of the full-length proteins produces well-defined polypeptide fragments (listed in Table 1). An aliquot of one protein's fragments is added to the aqueous phase bathing the *cis* side of a membrane that contains a single AeL nanopore, and a voltage V is applied across the membrane, which drives polypeptides into the pore nanopore one at a time, thereby causing brief but characteristic reductions in the pore's ionic current (Figure 1B). Three parameters for each event are recorded: the relative current blockade value (I_b/I_0, where I_0 and I_b are the ionic currents through a fully open and polypeptide-occupied pore, respectively), the dwell time of the molecule in the pore (t_b), and the ionic current standard deviation (σ_b) (Figure 1B).

The histograms of the relative current blockade values I_b/I_0 for each of the two cleaved protein fragments (Figure 1C) show that a single AeL nanopore can discriminate between the LysN-induced polypeptide fragments from full-length wild-type (αS_wt) and the point mutant (αS_E46K). In addition to the discriminatory capability of the I_b/I_0 histogram (Figure 1C), the proteins can also be qualitatively differentiated based on the dwell time- and standard deviation−event plot data (Figure S1, Supporting Information section).

In Figure 1C, there are fewer distinct peaks than one might expect based on the predicted action of the protease on the target protein. There are several hypothetical reasons that might account for that observation. First, proteolytic digestions are generally not 100% efficient in either the complete processing of the target protein or in the production of every polypeptide fragment. Second, it is possible that aggregation of either the target protein or some of the fragments could occur even though the experimental conditions (*i.e.*, a relatively short digestion time of 3 h, the pH was basic at pH 10, and no stirring was applied) are not conducive to that process (aggregated fragments would likely not enter the pore). Third, some of the predicted polypeptide fragments may not enter the pore due to an excessively high entropic cost (*i.e.*, their secondary structures may limit the partitioning of some polypeptides into the highly confined geometry of the nanopore). We are currently investigating this issue experimentally.

The green and red Gaussian fits to the single peaks in the I_b/I_0 histogram data (Figures 1C and S1) are located at I_b/I_0 = 0.34 ± 0.01 and 0.38 ± 0.01 for the samples derived from full-length (αS_wt) and (αS_E46K), respectively. Because the only polypeptide fragments that would contain the amino acids that are different in the two full-length proteins are $(\alpha S\_wt)_{13}$ and $(\alpha S\_E46K)_{12}$ (Tables 1 and 2), it follows that those particular fragments are the likely cause of those two different peaks.

To test that hypothesis, we studied the effects of synthetic polypeptides $(\alpha S\_wt)_{13}$ and $(\alpha S\_E46K)_{12}$ individually on the AeL nanopore. Figure 2A (top) shows that there is one peak in the I_b/I_0 histogram for $(\alpha S\_wt)_{13}$ located at 0.34 ± 0.01. The results obtained with $(\alpha S\_E46K)_{12}$ (Figure 2A, center) show that there are two peaks in its I_b/I_0 histogram: a predominant one located at 0.38 ± 0.01 and a secondary peak at 0.51 ± 0.01. Note that the locations of the single peak for $(\alpha S\_wt)_{13}$ and the more probable peak for $(\alpha S\_E46K)_{12}$ are situated at the same I_b/I_0 values as the Gaussian fit peaks from LysN-cleaved full-length (αS_wt) and (αS_E46K), respectively (Figure 1C). Note that the ionic current blockade dwell time (Figure 2B, center) and standard deviation (Figure 2C, center) *vs* the blockade depth (I_b/I_0) event plots provide two additional means to discriminate between these two synthetic polypeptides. Lastly, the bottom panels in Figure 2A−C show that the effects of $(\alpha S\_wt)_{13}$ and $(\alpha S\_E46K)_{12}$ on the AeL nanopore current are independent of each other, which suggests that the two different polypeptides do not interact significantly with each other in the bulk aqueous phase. The histograms shown in Figure 2, which were produced with equimolar concentrations of $(\alpha S\_wt)_{13}$ and $(\alpha S\_E46K)_{12}$ polypeptides, have qualitatively similar blockade event rates.

Table 3. Physical Properties of the Three 9-Amino-Acid-Long Polypeptides Predicted from LysN Cleavage of the Full-Length αS_wt Protein (from Table 1) and of the PTM Y39 Nitration Version[a]

Polypeptide Abbreviation	Sequence	Length (amino acids)	Mass (g mol^{-1})	Charge @ pH 7.5
(KE wt)	KEGVVAAAE	9	872.97	-1
(KG wt)	KQGVAEAAG	9	829.91	0
(Y39 wt)	KEGVLYVGS	9	951.09	0
(Y39 NO_2)	KEGVLY(NO_2)VGS	9	996.08	0

[a]The polypeptide abbreviations, which are specific to this study, are color-coded to aid interpretation of the electrophysiology data illustrated in Figure 3.

These results suggest that even though these two fragments are only slightly different in sequence, mass, and length (Table 2), the AeL nanopore can easily discriminate between them and thus between the LysN-cleaved versions of the full-length native and (αS_E46K) point mutant proteins (Figure 1).

Although the E46K point mutation correlates with some cases of PD and DLB, not all the patients affected by synucleinopathies present with it. Other reported neurodegenerative cases are associated with certain PTMs of αS. Thus, these PTMs, which include phosphorylation of S129,[64,65] nitration,[66] *O*-GlcNAcylation,[67] sumoylation, or ubiquitination,[66] are also used as biomarkers for PD and DLB.

LysN proteolysis of full-length αS_wt would theoretically produce three unique 9-amino-acid-long polypeptides (Table 1), which we label here as (KE wt), (KG wt), and (Y39 wt). The physical properties of those fragments and those of a Y39 nitration PTM of the latter one (Y39 NO_2) are listed in Table 3. Given that nanopores have proven useful for discriminating between different size RNA oligonucleotides,[45] synthetic polymers,[46,49] polypeptides,[68,69] and characterizing PTMs in proteins,[70−73] we tested whether the AeL nanopore can discriminate between these three identical-length wild-type protein fragments and a PTM nitration version.

Figure 3A−C shows the AeL nanopore electrophysiology data for the three 9-amino-acid-long polypeptide fragments predicted from LysN proteolysis of wild-type αS protein, each produce characteristic and differentiable distributions. The polypeptide fragment (KE wt) produces events characterized with one peak at I_b/I_0 = 0.48 ± 0.01 in the relative current blockade value histogram (Figure 3A left). Adding the (KG wt) polypeptide to the sample causes a new peak to appear at I_b/I_0 = 0.57 ± 0.02 (Figure 3B left). The subsequent addition of the third fragment type (Y39 wt) caused a broadening of the peak caused by (KE wt) due to an additional peak at I_b/I_0 = 0.49 ± 0.02 (Figure 3C left). Finally, adding the Y39 nitration PTM polypeptide (Y39 NO_2) caused another distinct peak at I_b/I_0 = 0.42 ± 0.02 (Figure 3D left).

While the I_b/I_0 histogram data allow the discrimination between all four of these polypeptides, their corresponding dwell time (t_b) event plots (Figure 3A−D, center) provide additional discriminatory capability. The latter plots show that the first two polypeptide variants, (KE wt) and (KG wt), have similar dwell time distributions with mean residence times $\langle t_b \rangle$ ∼ 0.3 and 0.5 ms, respectively (Figure 3B center). Both the third polypeptide variant (Y39 wt) and its Y39 nitration PTM version (Y39 NO2) have mean dwell times that, at $\langle t_b \rangle \approx 5.4$ and 7.9 ms, respectively, are about an order of magnitude longer than those for the other two polypeptides. Moreover, note that the clustered t_b event plots for each of the four variants are further distinguishable because their distributions cluster at different I_b/I_0 values. Moreover, the standard deviation (σ_b) event plots (Figure 3A to 3D right) for each variant are also distinct. Note further that the first three polypeptides (Figure 3C) are also discriminated when the whole αS protein variants discussed above are digested (Figures S2−S4 for αS_wt and S5 to S7 for αS_E46K).

Another relevant biomarker is a phosphorylation on serine residue S129. However, the length of the peptide fragment generated by LysN that includes S129 (Table 1) is longer than the pore's length and therefore not within the detectable and discernible length range for polypeptide discrimination with the AeL nanopore.[68,69] We overcame that limitation by changing the protease to cleave the relevant fragment into one that is sufficiently short. Specifically, we used another enzyme, AspN peptidyl-Asp metalloendopeptidase from the Gram-negative bacteria *Pseudomonas fragi*,[74−77] which cleaves at the amino terminus side of aspartic acid residues. This process should produce the polypeptide fragments listed in Table 4.

Our goal here was to determine whether the AeL nanopore can discriminate between wild-type αS and a PTM phosphorylation of serine residue at amino acid 129 (S129). AspN should produce a 14-amino-acid-long polypeptide that contains S129. This fragment and its phosphorylated version are listed in Table 5.

Figure 4 illustrates the AeL nanopore electrophysiology data for the (S129wt)AspN and phosphorylated PTM variant (S129_pho)AspN proteolysis fragments. The individual polypeptide fragment (S129_wt)AspN produces two peaks in the I_b/I_0 histogram at 0.18 ± 0.01 and 0.14 ± 0.01 (Figure 4A, left). The phosphorylated fragment (S129_pho)AspN produces also two peaks at I_b/I_0 = 0.20 ± 0.02 and 0.09 ± 0.01 (Figure 4B, left). When both polypeptides were detected with the AeL nanopore from a co-mixed sample, two well-defined populations were observed, which clearly show the pore's ability to discriminate between the minor components of (S129_wt)AspN and (S129_pho)AspN (Figure 4C, left). In addition, the dwell time (Figure 4A−C, center) and ionic current standard deviation (Figure 4A−C, right) event plots provided further discriminatory capability for this particular PTM. Note that the dominant peaks in the phosphorylation data overlap strongly. Nevertheless, the lesser peaks still provide a means to differentiate between the different species.

DISCUSSION

Previous studies on nanopore-based detection of individual polymers enabled sequencing DNA,[45,46,51,52,54,56] simultaneous detection of several different proteins,[78] discriminating between polymers based on their size,[46,49,53,57,79] and identifying several different proteins from their protease-induced fragments.[38,39,61] The work described herein represents a significant extension of the latter method. Specifically, we used two different proteases (LysN and AspN) and the AeL

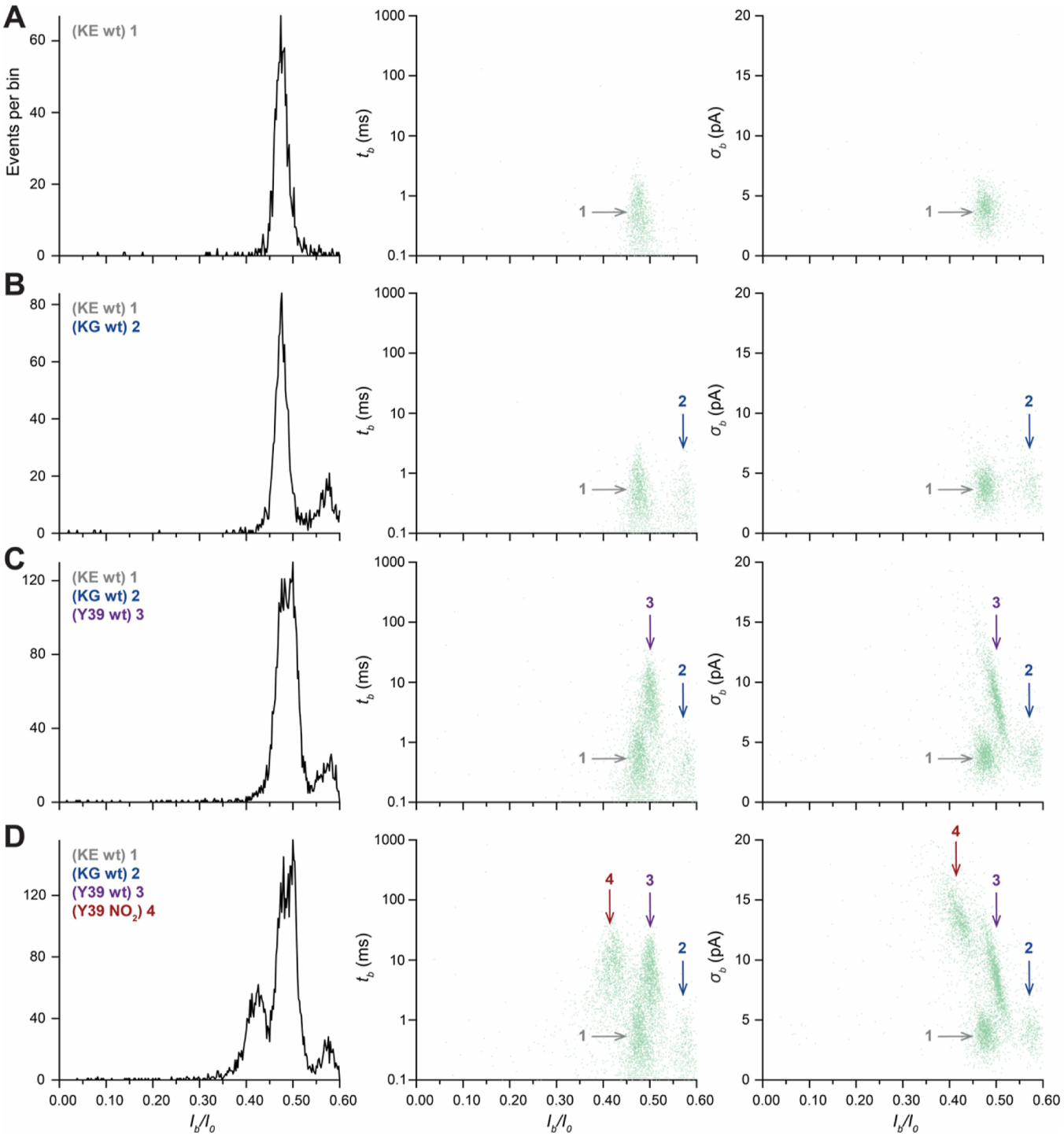

Figure 3. AeL nanopore-based discrimination of the three 9-amino-acid-long polypeptides predicted from LysN proteolysis of full-length αS_wt (Tables 1 and 3) and the PTM (Y39) nitration of one of the polymers (Table 3). The plots are histograms of the relative ionic current blockade value, I_b/I_0 (left), dwell time−current blockade value event plots (center), and ionic current standard deviation-current blockade value event plots (right) for a successive addition of (A) (KE wt), (B) (KE wt) + (KG wt), (C) (KE wt) + (KG wt) + (Y39 wt), and (D) (KE wt) + (KG wt) + (Y39 wt) + (Y39 NO_2). For clarity, the results that correspond to each polypeptide variant are indicated with arrows matching their respective color-code. The data shown is from a single experiment but was highly reproducible for $n > 3$ replicates.

nanopore to discriminate between wild-type α-Synuclein and three different versions of it (*i.e.*, a single-point mutation E46K and two different PTMs, Y39 nitration and S129 phosphorylation) that are implicated in several neurodegenerative diseases, including Parkinson's and DLB. The method shown here offers the possibility to detect various forms of proteins with a single nanopore through its versatility. This is made possible because of multiple selective proteases allow the precise cleavage of proteins into detectable and discriminable polypeptide fragments of the desired length bearing the mutation(s) or MTP(s) of interest.

We note that not all of the blockade events shown in Figure 1 are necessarily due to polypeptide translocation. Specifically, some of the events might instead be caused by polypeptides

Table 4. Seven Polypeptide Fragments Predicted from AspN Proteolysis of Full-Length Wild-Type αS Protein[a]

Length (amino acids)	Sequence	Mass (g mol^{-1})	Net Charge @ pH 7.5
1	M	149.21	0
2	DP	230.22	-1
4	DMPV	460.55	-1
6	DYEPEA	722.71	-3
14	DNEAYEMPSEEGYQ	1661.67	-5
17	DQLGKNEEGAPQEGILE	1826.94	-4
96	DVMMKGLSKAKEGVVAAAEKTKQGVAEAAGKTKEGV LYVGSKTKEGVVHGVATVAEKTKEQVTNVGGAVVTG VTAVAQKTVEGAGSIAAATGFVKK	9516.8	-5

[a]The 14-amino-acid-long variant, highlighted in yellow, and a phosphorylated variant of it (Table 5) were analyzed with a single AeL nanopore (Figure 4).

Table 5. Two Variants (Wild-Type and S129 Phosphorylation) of the Predicted 14-Amino-Acid-Long AspN-Cleaved Fragment from the Full-Length αS_wt Protein

Polypeptide	Length (amino acids)	Sequence	Mass (g mol^{-1})	Charge @ pH 7.5
(S129_wt)AspN	14	DNEAYEMPSEEGYQ	1661.67	-5
(S129_pho)AspN	14	DNEAYEMPS (pho) EEGYQ	1741.63	-7

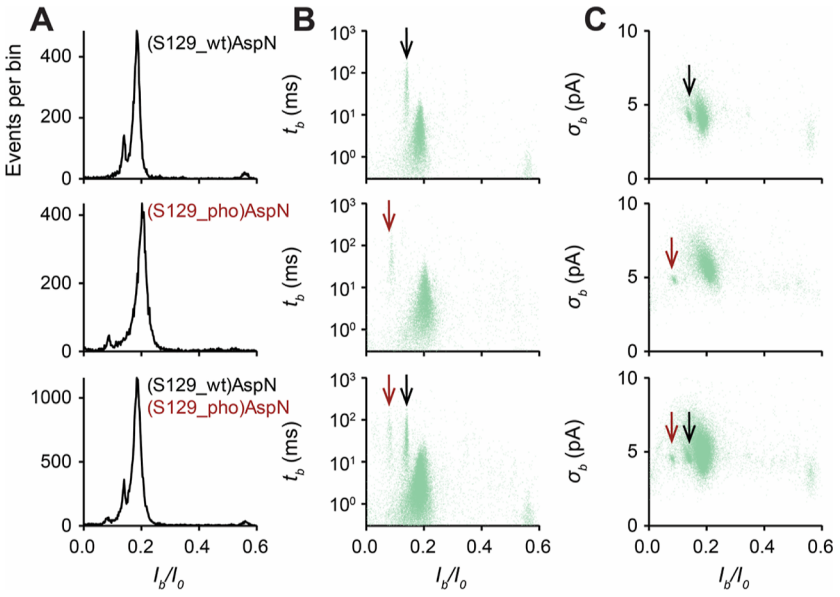

Figure 4. AeL nanopore-based discrimination of two 14-amino-acid-long polypeptides (αS_wt)AspN$_{14}$ and its phosphorylated version (αS_S129)AspN$_{14}$_pho. The single channel ionic current blockade value histograms (left), dwell time (t_b) *vs* current blockade value (I_b/I_0) event plots (center), and blocked ionic current standard deviation event plots (right) for (A) (S129_wt)AspN only, (B) (S129_pho)AspN only, or (C) a mixture of both (S129_wt)AspN and (S129_pho)AspN polypeptides in the same sample. For clarity, the results that correspond to each polypeptide variant are indicated with arrows matching their respective color-codes. All data were recorded at T = 22 °C, [KCl] = 2.5 M, [$CaCl_2$] = 1 M, [HEPES] = 25 mM, pH 7.5, and the transmembrane potential was V = +50 mV. The data shown are for single experiments but were highly reproducible in replicate (n > 3) experiments.

that enter and leave the pore from the sample side. Also, there are two known processes that can drive polypeptides into and possibly through the aerolysin channel. These include electrophoresis (*e.g.*, as was the case for single-stranded DNA transport through the αHL nanopore)[45] and electroosmosis, which can drive polypeptides with any net charge (positive, negative, or neutral) into and possibly through the pore.[39]

This method for the label-free identification of mutations and PTMs, which should work for many other proteins, could be a useful tool for rapid diagnoses at the point of care in medical facilities if it is integrated into a low-cost, miniaturized, high-throughput analytical platform. However, there are several technological hurdles and levels of systems integration (*e.g.*, of microfluidics-based protein separation,[80,81] *etc.*) that will need to be resolved or employed.

EXPERIMENTAL SECTION

Protein Synthesis. His SpinTrap mini columns were purchased from GE Healthcare Life Science (Chicago, IL, USA), IPTG (R0392), HEPES buffer (BP310) from Thermo Fisher Scientific (Waltham, MA, USA), and Vivaspin 10 kDa cut-off filters (VS0101) from Sartorius (Gottingen, Germany). LysN protease (L101) was purchased from ImmunoPrecise Antibodies (Victoria, Canada), trypsin-agarose (T1763), imidazole (104716), potassium chloride (P5405), calcium chloride (223506), trifluoroacetic acid (TFA, T6508), and decane (457116) were purchased from Merck (Darmstadt, Germany). Diphytanoyl-phosphocholine (DPhPC,

850356P) was purchased from Avanti Polar Lipids (Alabaster, AL, USA).

KEGVVHGVATVAE, KGVVHGVATVAE, KEGVVAAAE, KQGVAEAAG, KEGVYLVGS, KEGVY(NO_2)LVGS, DNEAYEMPSEEGYQ, and DNEAYEMPS(pho)EEGYQ polypeptides (purity ≥ 98%) were purchased from ProteoGenix (Schiltigheim, France), and recombinant αS_wt and αS_E46K (purity ≥ 95%) were purchased from rPeptide (Watkinsville, GA, USA).

Protein Digestion. Recombinant αS_wt and αS_E46K were dissolved in a 0.1 M glycine, 16 mM NaOH buffer at pH 10. The proteins were digested by LysN in a 1:50 ratio (protein/LysN, mass/mass) for 3 h at 37 °C. LysN cleavage was stopped by quenching the sample using 0.1% TFA. The subsequent fragmented proteins were filtered using a 10 kDa cut-off membrane at 15,000 x g 4 °C for 1 h to withdraw undigested, aggregated proteins, and native LysN protease. The fragmented samples were stored at -20 °C until their use.

Aerolysin Production. AeL is a pore-forming toxin from *A. hydrophila* produced as a precursor protein, proaerolysin (ProAeL), which forms soluble dimers. Recombinant wild-type ProAeL was produced in *Escherichia coli* BL21 using the pET22b-PA vector. ProAeL is produced after IPTG induction and localizes into the bacteria's periplasm. The periplasmic fraction containing soluble ProAeL dimers was extracted using an osmotic shock. Because the recombinant protein is C-terminal His-tagged, ProAeL was further purified by affinity chromatography using Ni-Sepharose MiniSpin columns, and elution was made by adding imidazole. The recombinant ProAeL purity (about 99%) was determined by SDS-polyacrylamide gel electrophoresis and Coomassie blue staining. The ProAeL concentration was estimated by optical absorbance at 280 nm. ProAeL (3 μg) was activated by 0.25 units of trypsin−agarose in 25 mM HEPES pH 7.5 for 30 min at 25 °C, as previously reported.[82]

***In Silico* Modeling of Protein Digestion.** While it is possible to predict which polypeptide fragments will be produced by LysN by inspection of the protein's sequence, we used an *in silico* fragmentation model of the αS protein that was calculated using the expasy PeptideCutter software (https://web.expasy.org/peptide_cutter/). The codes of αS_wt (P37840) and αS_E46K (P37840, VAR_022703) proteins are available in a free Uniprot database (https://www.uniprot.org).

Nanopore Recording. A vertical lipid bilayer electrophysiology setup (Warner Instruments, Hamden, CT, USA) was used for all the experiments with AeL. The lipid bilayer was formed by painting and spontaneous thinning a film of diphytanoyl-phosphocholine, DPhPC (Avanti Polar Lipids, Alabaster, AL, USA), in decane (Merck, Darmstadt, Germany) at 10 mg/mL over a 150 μm diameter aperture on a Teflon support separating the *cis*- and *trans*-compartments. The aqueous solutions on both sides of the membrane contained 1 mL of 2.5 M KCl 1 M $CaCl_2$, 25 mM HEPES at pH 7.5 (Merck, Darmstadt, Germany). Two matched Ag/AgCl electrodes (Alfa Aesar, Ward Hill, MA, USA) were used to apply +80 mV or +50 mV across the membrane and measure the ionic current. The *cis*-compartment is defined as the virtual ground. After forming the lipid bilayer, activated aerolysin was added to the *cis*-compartment at ≈ 50 ng/mL final concentration. Once a single AeL nanopore formed, a fragmented αS protein (αS_wt or αS_E46K digested by LysN) or an αS peptide sample was added to the *cis*-compartment. The final concentration of fragmented protein is 3.5 μM each of αS_wt and αS_E46K. The final concentration of (KE wt), (KG wt), (Y39 wt), and (Y39 NO2) polypeptides is 5 μM and for (S129_wt)AspN, (S129_pho)AspN is 30 μM.

Single-channel current recordings were performed using an Axopatch 200B patch-clamp amplifier (Molecular Devices, Sunnyvale, CA, USA) in the whole-cell mode with a CV-203BU headstage. The signal was filtered using the internal 4-pole Bessel filter at a cut-off frequency of 5 kHz. The data were digitized at 100 kHz and current digital resolution of 30.5 fA/bit state, using a DigiData 1550B A/D-converter (Molecular Devices) controlled by Clampex 10.2 software (Molecular Devices). The solution temperature was held at 22.0 ± 0.5 °C for all the experiments with a Peltier device controlled by a bipolar temperature controller (CL-100, Warner Instruments) coupled to a liquid cooling system (LCS-1, Warner Instruments).

Data Analysis. Data analysis was performed using Igor Pro 6.12A software (WaveMetrics, OR, USA) with in-house routines. The approach relies on a statistical analysis of the properties of the analyte-induced current blockades, involving at least several hundred (more typically thousands) events. The detection of each individual current blockade in a nanopore current *vs* time recording is based on a single current-threshold (*Th*) method. A blockade event is detected when the current magnitude becomes smaller than *Th*, until it returns to a value greater than *Th*. The beginning of the blockade is defined as the first point of current increase after having monotonically decreased below *Th*, and its end as the last point of current decrease before monotonically increasing above *Th*. This defines the range of points used to compute the characteristic quantities of the blockade, such as dwell time t_b, mean residual current value I_b, and the standard deviation σ_b of the residual current. Here, $Th = I_0 - 5\sigma_0$, where I_0 and σ_0 are the mean value and standard deviation of a Gaussian fit of the open-pore current distribution, respectively.

Histograms of the relative mean residual current I_b/I_0 are constructed with a bin width of 0.002. I_b/I_0 values constitute the main criterion to discriminate populations of blockades induced by enzymatically produced polypeptide fragments from the αS protein variants. I_b/I_0 population j is defined as the subset of blockades whose I_b/I_0 values fall in the range $\langle I_b/I_0\rangle_j \pm 1.96\sigma_j$, where $\langle I_b/I_0\rangle_j$ and σ_j are respectively the mean value and standard deviation of a Gaussian fit of the distribution of I_b/I_0 values in the corresponding histogram peak. This range includes 95% of the Gaussian distribution.

The mean blockade duration $\langle t_b\rangle_j$ is determined by fitting the distribution of $\ln[(t_b)_j]$ values with a single-exponential probability density model, where the maximum of the distribution occurs at $\ln[\langle t_b\rangle_j]$. The mean standard deviation of the residual current $\langle\sigma_b\rangle_j$ is the mean value of a Gaussian fit of the distribution of $(\sigma_b)_j$ values. In the case where the distribution of $(\sigma_b)_j$ presents different sub-populations, each sub-population is Gaussian-fitted and associated with its own mean value.

MALDI Instrumentation. MALDI-TOF mass spectra were acquired using a Bruker UltraFlextreme mass spectrometer (Bruker, Billerica, MA, USA) equipped with a Smartbeam 2 Nd/YAG laser (Bruker) operating at 355 nm. Spectra were acquired using FlexControl software (version 3.4 Bruker). The reflectron mode was used with a mass range of m/z 100 to 600. The fixed instrument voltages were ion source 1, 20.00 kV; ion source 2, 17.85 kV; lens, 7.90 kV; reflector 1, 20.80 kV; and reflector 2, 10.80 kV. All mass spectra were processed using FlexAnalysis software (version 3.4, Bruker). Pulsed ion extraction was set to 170 ns. Matrix suppression cut off mass was set to 500 m/z. Mass calibration was performed using peptide calibration standard from the Bruker Starter Kit (P/N 8208241).

MALDI Sample Preparation. The 2,5-dihydroxybenzoic acid (DHB) matrix was prepared at 20 mg/mL in 30% acetonitrile (v/v) in water with 0.1% trifluoroacetic acid (TFA). Polypeptides were diluted to a working concentration of 1 μM in 30% acetonitrile (v/v) in water with 0.1% TFA as well. Samples were mixed 1:1 with DHB matrix prior to spotting 1 μL on an MTP anchorchip 384 target (P/N 8280790) and allowed to air dry at room temperature.

■ ASSOCIATED CONTENT

Supporting Information

The Supporting Information is available free of charge at https://pubs.acs.org/doi/10.1021/acschemneuro.3c00164.

Discrimination between αS_wt and αS_E46K proteins; reproducibility of αS_wt protein fragmentation and $(\alpha S\_wt)_{13}$ identification; reproducibility of αS_E46K protein fragmentation and $(\alpha S\_E46K)_{12}$ identification;

MS analysis of αS_wt protein fragmentation; and MS analysis of αS_E46K protein fragmentation (PDF)

AUTHOR INFORMATION

Corresponding Authors

John J. Kasianowicz − *Dept. of Physics, University of South Florida, Tampa, Florida 33620, United States; Dept. of Applied Physics & Applied Mathematics, Columbia University, New York, New York 10027, United States; Freiburg Institute for Advanced Studies, Albert-Ludwigs Universität Freiburg, Freiburg 79104, Germany;* orcid.org/0000-0001-5106-7326; Phone: +1 (301) 250-8539; Email: jjkemail@mac.com

Abdelghani Oukhaled − *CY Cergy Paris Université, CNRS, LAMBE, Cergy 95000, France;* orcid.org/0000-0002-9675-6747; Phone: +33 01 34 25 65 71; Email: abdelghani.oukhaled@cyu.fr

Authors

Mazdak Afshar Bakshloo − *CY Cergy Paris Université, CNRS, LAMBE, Cergy 95000, France*

Safia Yahiaoui − *CY Cergy Paris Université, CNRS, LAMBE, Cergy 95000, France*

Matthieu Bourderioux − *Université Paris-Saclay, Univ Evry, CNRS, LAMBE, Evry-Courcouronnes 91025, France*

Regis Daniel − *Université Paris-Saclay, Univ Evry, CNRS, LAMBE, Evry-Courcouronnes 91025, France;* orcid.org/0000-0003-0725-5439

Manuela Pastoriza-Gallego − *CY Cergy Paris Université, CNRS, LAMBE, Cergy 95000, France*

Complete contact information is available at: https://pubs.acs.org/10.1021/acschemneuro.3c00164

Author Contributions

M.A.B., J.J.K., and A.O. conceived the project, designed the experiments, organized and wrote the manuscript. S.Y. and M.A.B. performed the nanopore experiments. M.A.B. analyzed the data from the nanopore experiments. M.B., R.D., and M.A.B. conceived mass spectrometry experiments and analyzed data from them. M.P.G. and M.A.B. elaborated the protocol of αS enzymatic degradation. M.P.G. produced the aerolysin nanopore material.

Notes

The authors declare no competing financial interest.

ACKNOWLEDGMENTS

This work was supported in part by the Agence Nationale de la Recherche ANR (ANR-17-CE09-0032-01 to A.O.), the NIST Office of Law Enforcement Standards, and a Marie Skłodowska-Curie/Freiburg Institute for Advanced Studies Senior Fellowship (both to J.J.K.). We thank F. Gisou van der Goot (Ecole Polytechnique Federale de Lausanne, Switzerland) for providing the pET22b-proAL plasmid containing the pro-aerolysin sequence.

ABBREVIATIONS

αS, alpha synuclein; DLB, dementia with Lewy bodies; PD, Parkinson's disease; AeL, Aerolysin; PTM, post-translational modification; KCl, potassium chloride; $CaCl_2$, calcium chloride

REFERENCES

(1) Maroteaux, L.; Campanelli, J.; Scheller, R. Synuclein: a neuron-specific protein localized to the nucleus and presynaptic nerve terminal. *J. Neurosci.* **1988**, *8*, 2804−2815.

(2) Maroteaux, L.; Scheller, R. H. The Rat Brain Synucleins; Family of Proteins Transiently Associated with Neuronal Membrane. *Mol. Brain Res.* **1991**, *11*, 335−343.

(3) Taguchi, K.; Watanabe, Y.; Tsujimura, A.; Tanaka, M. Brain Region-Dependent Differential Expression of Alpha-Synuclein. *J. Comp. Neurol.* **2016**, *524*, 1236−1258.

(4) Bendor, J. T.; Logan, T. P.; Edwards, R. H. The Function of α-Synuclein. *Neuron* **2013**, *79*, 1044−1066.

(5) Huang, C.-C.; Chiu, T.-Y.; Lee, T.-Y.; Hsieh, H.-J.; Lin, C.-C.; Kao, L.-S. Soluble α-synuclein facilitates priming and fusion by releasing Ca2+ from thapsigargin-sensitive Ca2+ pool in PC12 cells. *J. Cell Sci.* **2018**, *131*, jcs213017.

(6) Lee, V. M.-Y.; Trojanowski, J. Q. Mechanisms of Parkinson's Disease Linked to Pathological α-Synuclein: New Targets for Drug Discovery. *Neuron* **2006**, *52*, 33−38.

(7) Stefanis, L. α-Synuclein in Parkinson's Disease. *Cold Spring Harbor Perspect. Med.* **2012**, *2*, a009399.

(8) Graham, J. G.; Oppenheimer, D. R. Orthostatic Hypotension and Nicotine Sensitivity in a Case of Multiple System Atrophy. *J. Neurol. Neurosurg. Psychiatry* **1969**, *32*, 28−34.

(9) Stefanova, N.; Bücke, P.; Duerr, S.; Wenning, G. K. Multiple System Atrophy: An Update. *Lancet Neurol.* **2009**, *8*, 1172−1178.

(10) Wenning, G. K.; Stefanova, N. Recent Developments in Multiple System Atrophy. *J. Neurol.* **2009**, *256*, 1791−1808.

(11) Laurens, B.; Vergnet, S.; Lopez, M. C.; Foubert-Samier, A.; Tison, F.; Fernagut, P.-O.; Meissner, W. G. Multiple System Atrophy - State of the Art. *Curr. Neurol. Neurosci. Rep.* **2017**, *17*, 41.

(12) Spillantini, M. G.; Schmidt, M. L.; Lee, V. M.-Y.; Trojanowski, J. Q.; Jakes, R.; Goedert, M. α-Synuclein in Lewy bodies. *Nature* **1997**, *388*, 839−840.

(13) Kim, W. S.; Kågedal, K.; Halliday, G. M. Alpha-Synuclein Biology in Lewy Body Diseases. *Alzheimer's Research & Therapy* **2014**, *6*, 73.

(14) Simon, C.; Soga, T.; Okano, H. J.; Parhar, I. α-Synuclein-mediated neurodegeneration in Dementia with Lewy bodies: the pathobiology of a paradox. *Cell Biosci.* **2021**, *11*, 196.

(15) Marotta, N. P.; Ara, J.; Uemura, N.; Lougee, M. G.; Meymand, E. S.; Zhang, B.; Petersson, E. J.; Trojanowski, J. Q.; Lee, V. M.-Y. Alpha-Synuclein from Patient Lewy Bodies Exhibits Distinct Pathological Activity That Can Be Propagated in Vitro. *Acta Neuropathol. Commun.* **2021**, *9*, 188.

(16) Ayers, J. I.; Lee, J.; Monteiro, O.; Woerman, A. L.; Lazar, A. A.; Condello, C.; Paras, N. A.; Prusiner, S. B. Different α-synuclein prion strains cause dementia with Lewy bodies and multiple system atrophy. *Proc. Natl. Acad. Sci. U.S.A.* **2022**, *119*, No. e2113489119.

(17) George, J. M. The Synucleins. *Genome Biol.* **2002**, *3*, REVIEWS3002.

(18) Goedert, M.; Jakes, R.; Spillantini, M. G. The Synucleinopathies: Twenty Years On. *JPD* **2017**, *7*, S51−S69.

(19) Esteban-Martín, S.; Silvestre-Ryan, J.; Bertoncini, C. W.; Salvatella, X. Identification of Fibril-Like Tertiary Contacts in Soluble Monomeric α-Synuclein. *Biophys. J.* **2013**, *105*, 1192−1198.

(20) Vilar, M.; Chou, H.-T.; Lührs, T.; Maji, S. K.; Riek-Loher, D.; Verel, R.; Manning, G.; Stahlberg, H.; Riek, R. The fold of α-synuclein fibrils. *Proc. Natl. Acad. Sci. U.S.A.* **2008**, *105*, 8637−8642.

(21) Cremades, N.; Cohen, S. I. A.; Deas, E.; Abramov, A. Y.; Chen, A. Y.; Orte, A.; Sandal, M.; Clarke, R. W.; Dunne, P.; Aprile, F. A.; Bertoncini, C. W.; Wood, N. W.; Knowles, T. P. J.; Dobson, C. M.; Klenerman, D. Direct Observation of the Interconversion of Normal and Toxic Forms of α-Synuclein. *Cell* **2012**, *149*, 1048−1059.

(22) Lorenzen, N.; Lemminger, L.; Pedersen, J. N.; Nielsen, S. B.; Otzen, D. E. The N-terminus of α-synuclein is essential for both monomeric and oligomeric interactions with membranes. *FEBS Lett.* **2014**, *588*, 497−502.

(23) Guerrero-Ferreira, R.; Taylor, N. M.; Mona, D.; Ringler, P.; Lauer, M. E.; Riek, R.; Britschgi, M.; Stahlberg, H. Cryo-EM Structure of Alpha-Synuclein Fibrils. *eLife* **2018**, *7*, No. e36402.
(24) Guerrero-Ferreira, R.; Kovacik, L.; Ni, D.; Stahlberg, H. New Insights on the Structure of Alpha-Synuclein Fibrils Using Cryo-Electron Microscopy. *Curr. Opin. Neurobiol.* **2020**, *61*, 89−95.
(25) Mandal, P. K.; Pettegrew, J. W.; Masliah, E.; Hamilton, R. L.; Mandal, R. Interaction between Aβ Peptide and α Synuclein: Molecular Mechanisms in Overlapping Pathology of Alzheimer's and Parkinson's in Dementia with Lewy Body Disease. *Neurochem. Res.* **2006**, *31*, 1153−1162.
(26) Chen, G.; Xu, T.; Yan, Y.; Zhou, Y.; Jiang, Y.; Melcher, K.; Xu, H. E. Amyloid Beta: Structure, Biology and Structure-Based Therapeutic Development. *Acta Pharmacol. Sin.* **2017**, *38*, 1205−1235.
(27) Uéda, K.; Fukushima, H.; Masliah, E.; Xia, Y.; Iwai, A.; Yoshimoto, M.; Otero, D. A.; Kondo, J.; Ihara, Y.; Saitoh, T. Molecular Cloning of CDNA Encoding an Unrecognized Component of Amyloid in Alzheimer Disease. *Proc. Natl. Acad. Sci. U.S.A.* **1993**, *90*, 11282−11286.
(28) Touchman, J. W.; Dehejia, A.; Chiba-Falek, O.; Cabin, D. E.; Schwartz, J. R.; Orrison, B. M.; Polymeropoulos, M. H.; Nussbaum, R. L. Human and Mouse α-Synuclein Genes: Comparative Genomic Sequence Analysis and Identification of a Novel Gene Regulatory Element. *Genome Res.* **2001**, *11*, 78.
(29) Gitler, A. D.; Chesi, A.; Geddie, M. L.; Strathearn, K. E.; Hamamichi, S.; Hill, K. J.; Caldwell, K. A.; Caldwell, G. A.; Cooper, A. A.; Rochet, J.-C.; Lindquist, S. α-Synuclein is part of a diverse and highly conserved interaction network that includes PARK9 and manganese toxicity. *Nat. Genet.* **2009**, *41*, 308−315.
(30) Xia, K.; Hagan, J. T.; Fu, L.; Sheetz, B. S.; Bhattacharya, S.; Zhang, F.; Dwyer, J. R.; Linhardt, R. J. Synthetic Heparan Sulfate Standards and Machine Learning Facilitate the Development of Solid-State Nanopore Analysis. *Proc. Natl. Acad. Sci. U.S.A.* **2021**, *118*, No. e2022806118.
(31) Uversky, V. N.; Fink, A. L. Amino acid determinants of α-synuclein aggregation: putting together pieces of the puzzle. *FEBS Lett.* **2002**, *522*, 9−13.
(32) Polymeropoulos, M. H.; Lavedan, C.; Leroy, E.; Ide, S. E.; Dehejia, A.; Dutra, A.; Pike, B.; Root, H.; Rubenstein, J.; Boyer, R.; Stenroos, E. S.; Chandrasekharappa, S.; Athanassiadou, A.; Papapetropoulos, T.; Johnson, W. G.; Lazzarini, A. M.; Duvoisin, R. C.; Di Iorio, G.; Golbe, L. I.; Nussbaum, R. L. Mutation in the α-Synuclein Gene Identified in Families with Parkinson's Disease. *Science* **1997**, *276*, 2045−2047.
(33) Ki, C.-S.; Stavrou, E.; Davanos, N.; Lee, W.; Chung, E.; Kim, J.-Y.; Athanassiadou, A. The Ala53Thr mutation in the α-synuclein gene in a Korean family with Parkinson disease. *Clin. Genet.* **2007**, *71*, 471−473.
(34) Puschmann, A.; Ross, O. A.; Vilariño-Güell, C.; Lincoln, S. J.; Kachergus, J. M.; Cobb, S. A.; Lindquist, S. G.; Nielsen, J. E.; Wszolek, Z. K.; Farrer, M.; Widner, H.; van Westen, D.; Hägerström, D.; Markopoulou, K.; Chase, B. A.; Nilsson, K.; Reimer, J.; Nilsson, C. A Swedish family with de novo α-synuclein A53T mutation: Evidence for early cortical dysfunction. *Parkinsonism Relat. Disorders* **2009**, *15*, 627−632.
(35) Pasanen, P.; Myllykangas, L.; Siitonen, M.; Raunio, A.; Kaakkola, S.; Lyytinen, J.; Tienari, P. J.; Pöyhönen, M.; Paetau, A. A novel α-synuclein mutation A53E associated with atypical multiple system atrophy and Parkinson's disease-type pathology. *Neurobiol. Aging* **2014**, *35*, 2180.e1−2180.e5.
(36) Krüger, R.; Kuhn, W.; Müller, T.; Woitalla, D.; Graeber, M.; Kösel, S.; Przuntek, H.; Epplen, J. T.; Schols, L.; Riess, O. AlaSOPro mutation in the gene encoding α-synuclein in Parkinson's disease. *Nat. Genet.* **1998**, *18*, 106−108.
(37) Zarranz, J. J.; Alegre, J.; Gómez-Esteban, J. C.; Lezcano, E.; Ros, R.; Ampuero, I.; Vidal, L.; Hoenicka, J.; Rodriguez, O.; Atarés, B.; Llorens, V.; Tortosa, E. G.; del Ser, T.; Muñoz, D. G.; de Yebenes, J. G. The new mutation, E46K, of α-synuclein causes parkinson and Lewy body dementia: New α-Synuclein Gene Mutation. *Ann. Neurol.* **2004**, *55*, 164−173.
(38) Afshar Bakshloo, M.; Kasianowicz, J. J.; Pastoriza-Gallego, M.; Mathé, J.; Daniel, R.; Piguet, F.; Oukhaled, A. Nanopore-Based Protein Identification. *J. Am. Chem. Soc.* **2022**, *144*, 2716−2725.
(39) Bakshloo, M. A.; Yahiaoui, S.; Piguet, F.; Pastoriza-Gallego, M.; Daniel, R.; Mathé, J.; Kasianowicz, J. J.; Oukhaled, A. Polypeptide Analysis for Nanopore-Based Protein Identification. *Nano Res.* **2022**, *15*, 9831−9842.
(40) Hohmann, L.; Sherwood, C.; Eastham, A.; Peterson, A.; Eng, J. K.; Eddes, J. S.; Shteynberg, D.; Martin, D. B. Proteomic Analyses Using Grifola Frondosa Metalloendoprotease Lys-N. *J. Proteome Res.* **2009**, *8*, 1415−1422.
(41) Tsiatsiani, L.; Heck, A. J. R. Proteomics beyond Trypsin. *FEBS J.* **2015**, *282*, 2612−2626.
(42) Zhao, M.; Hao, B.; Li, H.; Cai, M.; Xie, J.; Liu, H.; Tan, M.; Zhai, L.; Yu, Q. Peptidyl-Lys Metalloendopeptidase (Lys-N) Purified from Dry Fruit of Grifola Frondosa Demonstrates "Mirror"Digestion Property with Lysyl Endopeptidase (Lys-C). *Rapid Commun. Mass Spectrom.* **2020**, *34*, No. e8573.
(43) Bezrukov, S. M.; Kasianowicz, J. J. Current Noise Reveals Protonation Kinetics and Number of Ionizable Sites in an Open Protein Ion Channel. *Phys. Rev. Lett.* **1993**, *70*, 2352−2355.
(44) Kasianowicz, J. J.; Bezrukov, S. M. Protonation Dynamics of the Alpha-Toxin Ion Channel from Spectral Analysis of PH-Dependent Current Fluctuations. *Biophys. J.* **1995**, *69*, 94−105.
(45) Kasianowicz, J. J.; Brandin, E.; Branton, D.; Deamer, D. W. Characterization of Individual Polynucleotide Molecules Using a Membrane Channel. *Proc. Natl. Acad. Sci. U.S.A.* **1996**, *93*, 13770−13773.
(46) Robertson, J. W. F.; Rodrigues, C. G.; Stanford, V. M.; Rubinson, K. A.; Krasilnikov, O. V.; Kasianowicz, J. J. Single-Molecule Mass Spectrometry in Solution Using a Solitary Nanopore. *Proc. Natl. Acad. Sci. U.S.A.* **2007**, *104*, 8207−8211.
(47) Kasianowicz, J. J.; Robertson, J. W. F.; Chan, E. R.; Reiner, J. E.; Stanford, V. M. Nanoscopic Porous Sensors. *Annual Rev. Anal. Chem.* **2008**, *1*, 737−766.
(48) Howorka, S.; Siwy, Z. Nanopore Analytics: Sensing of Single Molecules. *Chem. Soc. Rev.* **2009**, *38*, 2360.
(49) Reiner, J. E.; Kasianowicz, J. J.; Nablo, B. J.; Robertson, J. W. F. Theory for Polymer Analysis Using Nanopore-Based Single-Molecule Mass Spectrometry. *Proc. Natl. Acad. Sci. U.S.A.* **2010**, *107*, 12080−12085.
(50) Schibel, A. E. P.; An, N.; Jin, Q.; Fleming, A. M.; Burrows, C. J.; White, H. S. Nanopore Detection of 8-Oxo-7,8-Dihydro-2′-Deoxyguanosine in Immobilized Single-Stranded DNA via Adduct Formation to the DNA Damage Site. *J. Am. Chem. Soc.* **2010**, *132*, 17992−17995.
(51) Derrington, I. M.; Butler, T. Z.; Collins, M. D.; Manrao, E.; Pavlenok, M.; Niederweis, M.; Gundlach, J. H. Nanopore DNA Sequencing with MspA. *Proc. Natl. Acad. Sci. U.S.A.* **2010**, *107*, 16060−16065.
(52) Manrao, E. A.; Derrington, I. M.; Laszlo, A. H.; Langford, K. W.; Hopper, M. K.; Gillgren, N.; Pavlenok, M.; Niederweis, M.; Gundlach, J. H. Reading DNA at Single-Nucleotide Resolution with a Mutant MspA Nanopore and Phi29 DNA Polymerase. *Nat. Biotechnol.* **2012**, *30*, 349−353.
(53) Baaken, G.; Ankri, N.; Schuler, A.-K.; Rühe, J.; Behrends, J. C. Nanopore-Based Single-Molecule Mass Spectrometry on a Lipid Membrane Microarray. *ACS Nano* **2011**, *5*, 8080−8088.
(54) Kumar, S.; Tao, C.; Chien, M.; Hellner, B.; Balijepalli, A.; Robertson, J. W. F.; Li, Z.; Russo, J. J.; Reiner, J. E.; Kasianowicz, J. J.; Ju, J. PEG-Labeled Nucleotides and Nanopore Detection for Single Molecule DNASequencing by Synthesis. *Sci. Rep.* **2012**, *2*, 684.
(55) Baaken, G.; Halimeh, I.; Bacri, L.; Pelta, J.; Oukhaled, A.; Behrends, J. C. High-Resolution Size-Discrimination of Single Nonionic Synthetic Polymers with a Highly Charged Biological Nanopore. *ACS Nano* **2015**, *9*, 6443−6449.

(56) Fuller, C. W.; Kumar, S.; Porel, M.; Chien, M.; Bibillo, A.; Stranges, P. B.; Dorwart, M.; Tao, C.; Li, Z.; Guo, W.; Shi, S.; Korenblum, D.; Trans, A.; Aguirre, A.; Liu, E.; Harada, E. T.; Pollard, J.; Bhat, A.; Cech, C.; Yang, A.; Arnold, C.; Palla, M.; Hovis, J.; Chen, R.; Morozova, I.; Kalachikov, S.; Russo, J. J.; Kasianowicz, J. J.; Davis, R.; Roever, S.; Church, G. M.; Ju, J. Real-Time Single-Molecule Electronic DNA Sequencing by Synthesis Using Polymer-Tagged Nucleotides on a Nanopore Array. *Proc. Natl. Acad. Sci. U.S.A.* **2016**, *113*, 5233−5238.

(57) Piguet, F.; Ouldali, H.; Discala, F.; Breton, M.-F.; Behrends, J. C.; Pelta, J.; Oukhaled, A. High Temperature Extends the Range of Size Discrimination of Nonionic Polymers by a Biological Nanopore. *Sci. Rep.* **2016**, *6*, 38675.

(58) Talarimoghari, M.; Baaken, G.; Hanselmann, R.; Behrends, J. C. Size-Dependent Interaction of a 3-Arm Star Poly(Ethylene Glycol) with Two Biological Nanopores. *Eur. Phys. J. E* **2018**, *41*, 77.

(59) Manrao, E. A.; Derrington, I. M.; Pavlenok, M.; Niederweis, M.; Gundlach, J. H. Nucleotide Discrimination with DNA Immobilized in the MspA Nanopore. *PLoS One* **2011**, *6*, No. e25723.

(60) Wang, H.; Ettedgui, J.; Forstater, J.; Robertson, J. W. F.; Reiner, J. E.; Zhang, H.; Chen, S.; Kasianowicz, J. J. Determining the Physical Properties of Molecules with Nanometer-Scale Pores. *ACS Sens.* **2018**, *3*, 251−263.

(61) Lucas, F. L. R.; Versloot, R. C. A.; Yakovlieva, L.; Walvoort, M. T. C.; Maglia, G. Protein Identification by Nanopore Peptide Profiling. *Nat. Commun.* **2021**, *12*, 5795.

(62) Parker, M. W.; Buckley, J. T.; Postma, J. P. M.; Tucker, A. D.; Leonard, K.; Pattus, F.; Tsernoglou, D. Structure of the Aeromonas toxin proaerolysin in its water-soluble and membrane-channel states. *Nature* **1994**, *367*, 292−295.

(63) Degiacomi, M. T.; Iacovache, I.; Pernot, L.; Chami, M.; Kudryashev, M.; Stahlberg, H.; van der Goot, F. G.; Dal Peraro, M. Molecular Assembly of the Aerolysin Pore Reveals a Swirling Membrane-Insertion Mechanism. *Nat. Chem. Biol.* **2013**, *9*, 623−629.

(64) Vicente Miranda, H.; Cássio, R.; Correia-Guedes, L.; Gomes, M. A.; Chegão, A.; Miranda, E.; Soares, T.; Coelho, M.; Rosa, M. M.; Ferreira, J. J.; Outeiro, T. F. Posttranslational Modifications of Blood-Derived Alpha-Synuclein as Biochemical Markers for Parkinson's Disease. *Sci. Rep.* **2017**, *7*, 13713.

(65) Levine, P. M.; Galesic, A.; Balana, A. T.; Mahul-Mellier, A.-L.; Navarro, M. X.; De Leon, C. A.; Lashuel, H. A.; Pratt, M. R. α-Synuclein O-GlcNAcylation alters aggregation and toxicity, revealing certain residues as potential inhibitors of Parkinson's disease. *Proc. Natl. Acad. Sci. U.S.A.* **2019**, *116*, 1511−1519.

(66) Wang, Y.; Shi, M.; Chung, K. A.; Zabetian, C. P.; Leverenz, J. B.; Berg, D.; Srulijes, K.; Trojanowski, J. Q.; Lee, V. M.-Y.; Siderowf, A. D.; Hurtig, H.; Litvan, I.; Schiess, M. C.; Peskind, E. R.; Masuda, M.; Hasegawa, M.; Lin, X.; Pan, C.; Galasko, D.; Goldstein, D. S.; Jensen, P. H.; Yang, H.; Cain, K. C.; Zhang, J. Phosphorylated α-Synuclein in Parkinson's Disease. *Sci. Transl. Med.* **2012**, *4*, 121ra20.

(67) Anderson, J. P.; Walker, D. E.; Goldstein, J. M.; de Laat, R.; Banducci, K.; Caccavello, R. J.; Barbour, R.; Huang, J.; Kling, K.; Lee, M.; Diep, L.; Keim, P. S.; Shen, X.; Chataway, T.; Schlossmacher, M. G.; Seubert, P.; Schenk, D.; Sinha, S.; Gai, W. P.; Chilcote, T. J. Phosphorylation of Ser-129 Is the Dominant Pathological Modification of α-Synuclein in Familial and Sporadic Lewy Body Disease. *J. Biol. Chem.* **2006**, *281*, 29739−29752.

(68) Piguet, F.; Ouldali, H.; Pastoriza-Gallego, M.; Manivet, P.; Pelta, J.; Oukhaled, A. Identification of Single Amino Acid Differences in Uniformly Charged Homopolymeric Peptides with Aerolysin Nanopore. *Nat. Commun.* **2018**, *9*, 966.

(69) Ouldali, H.; Sarthak, K.; Ensslen, T.; Piguet, F.; Manivet, P.; Pelta, J.; Behrends, J. C.; Aksimentiev, A.; Oukhaled, A. Electrical Recognition of the Twenty Proteinogenic Amino Acids Using an Aerolysin Nanopore. *Nat. Biotechnol.* **2020**, *38*, 176−181.

(70) Rosen, C. B.; Rodriguez-Larrea, D.; Bayley, H. Single-Molecule Site-Specific Detection of Protein Phosphorylation with a Nanopore. *Nat. Biotechnol.* **2014**, *32*, 179−181.

(71) Restrepo-Pérez, L.; Huang, G.; Bohländer, P. R.; Worp, N.; Eelkema, R.; Maglia, G.; Joo, C.; Dekker, C. Resolving Chemical Modifications to a Single Amino Acid within a Peptide Using a Biological Nanopore. *ACS Nano* **2019**, *13*, 13668−13676.

(72) Li, S.; Wu, X.; Li, M.; Liu, S.; Ying, Y.; Long, Y. T232K/K238Q Aerolysin Nanopore for Mapping Adjacent Phosphorylation Sites of a Single Tau Peptide. *Small Methods* **2020**, *4*, 2000014.

(73) Ensslen, T.; Sarthak, K.; Aksimentiev, A.; Behrends, J. C. Resolving Isomeric Posttranslational Modifications Using a Biological Nanopore as a Sensor of Molecular Shape. *J. Am. Chem. Soc.* **2022**, *144*, 16060−16068.

(74) Porzio, M. A.; Pearson, A. M. Isolation of an Extracellular Neutral Proteinase from Pseudomonas Fragi. *Biochim. Biophys. Acta Enzymol.* **1975**, *384*, 235−241.

(75) Noreau, J.; Drapeau, G. R. Isolation and Properties of the Protease from the Wild-Type and Mutant Strains of Pseudomonas Fragi. *J. Bacteriol.* **1979**, *140*, 911−916.

(76) Drapeau, G. R. Substrate Specificity of a Proteolytic Enzyme Isolated from a Mutant of Pseudomonas Fragi. *J. Biol. Chem.* **1980**, *255*, 839−840.

(77) Hagmann, M.-L.; Geuss, U.; Fischer, S.; Kresse, G.-B. [51] Peptidyl-Asp Metalloendopeptidase. *Methods in Enzymology*; Academic Press, 1995; Vol. *248*, pp 782−787.

(78) Kasianowicz, J. J.; Henrickson, S. E.; Weetall, H. H.; Robertson, B. Simultaneous Multianalyte Detection with a Nanometer-Scale Pore. *Anal. Chem.* **2001**, *73*, 2268−2272.

(79) Rodrigues, C. G.; Machado, D. C.; Chevtchenko, S. F.; Krasilnikov, O. V. Mechanism of KCl Enhancement in Detection of Nonionic Polymers by Nanopore Sensors. *Biophys. J.* **2008**, *95*, 5186−5192.

(80) Ramsey, J. D.; Jacobson, S. C.; Culbertson, C. T.; Ramsey, J. M. High-Efficiency, Two-Dimensional Separations of Protein Digests on Microfluidic Devices. *Anal. Chem.* **2003**, *75*, 3758−3764.

(81) Foote, R. S.; Khandurina, J.; Jacobson, S. C.; Ramsey, J. M. Preconcentration of Proteins on Microfluidic Devices Using Porous Silica Membranes. *Anal. Chem.* **2005**, *77*, 57−63.

(82) Afshar Bakshloo, M.; Yahiaoui, S.; Ouldali, H.; Pastoriza-Gallego, M.; Piguet, F.; Oukhaled, A. On Possible Trypsin-induced Biases in Peptides Analysis with Aerolysin Nanopore. *Proteomics* **2022**, *22*, 2100056.